RSC Advances

PAPER

View Article Online
View Journal | View Issue

Cite this: *RSC Adv.*, 2021, **11**, 29816

Investigating conjugated polymer nanoparticle formulations for lateral flow immunoassays†

Moritz Schüller,[a] Annette Meister,[b] Mark Green [c] and Lea Ann Dailey *[d]

Lateral flow immunoassays (LFI) are valuable tools for point-of-care testing. However, their sensitivity is limited and can be further improved. Nanoparticles (NP) of conjugated polymers (CPNs), also known as Pdots, are reported to be highly sensitive fluorescent probes, but a direct comparison with conventional colloidal gold-based (Au-NP) LFI using the same antibody–antigen pair is missing to date. Furthermore, the influence of brightness and Stokes shift of CPs on the signal : background ratio (SBR) needs to be evaluated. In this study, we encapsulated two different CPs, poly-(9,9-di-*n*-octyl-fluorenyl-2,7-diyl) (PDOF) and poly-(2,5-di-hexyloxy-cyanoterephthalylidene) (CN-PPV) in silica shell-crosslinked Pluronic© micelles (Si-NP) and Pdots and investigated the NP brightness with respect to CP loading dose. The brightest formulation of each NP system was conjugated to rabbit IgG as a model antigen and the SBR was investigated in an ELISA-like microplate assay and LFI. Two reference particles, Au-NP and a polystyrene NP (PS-NP) loaded with a small-molecule fluorescent dye were conjugated to IgG and compared to the Si-NP and Pdots. The mass of Pdots required for detection in LFI was at least two orders of magnitude lower than that of Si-NP and the reference NP. The SBR of CN-PPV (moderate brightness, large Stokes shift) was two to three times higher than the SBR of PDOF (high brightness, small Stokes shift). To combine the favourable properties of both CPs, a polymer blend of PDOF and CN-PPV was encapsulated in Pdots, and resulted in further increase of SBR in the microplate assay and LFI. In summary, combining two CPs with different properties can lead to fluorescent signal-transducers for applications such as ELISA and LFIs, which can enhance the detection limit of the assay by 2–3 orders of magnitude.

Received 6th July 2021
Accepted 17th August 2021

DOI: 10.1039/d1ra05212h

rsc.li/rsc-advances

Introduction

Between December 2019 and 2020, the COVID-19 pandemic caused 79.2 million cases of infection and 1.7 million deaths worldwide.[1] As a vital part of the worldwide countermeasures, a vast number of the population is tested for the infection every day. It has been shown that a negative correlation between the number of tests per inhabitant and mortality exists,[2] indicating that a higher testing rate could decrease the number of infections and mortality rate.

The most inexpensive and rapid test method is the lateral flow immunoassay (LFI), but the sensitivity of these assays is not as high as alternative methods, such as real-time polymerase chain reaction (RT-PCR).[3] Most LFI assays are based on the visual evaluation of a colored nanoparticle (NP) probe, usually colloidal gold nanoparticles (Au-NP), which accumulate on the test or control line of the membrane, thereby becoming visually detectable through their red color.[4] A substantial increase in sensitivity can be achieved by fluorescent NP signal transducers and the first over-the-counter assay for COVID-19 to receive the FDA emergency approval was a quantum dot-based fluorescent LFI.[5] However, quantum dots are usually made from elements like Ga, Se, Cd, Te, In and Hg,[6] These elements are 100–1000 times less abundant in accessible earth crust compared to carbon, thus more expensive.[7] The toxicity of these components is furthermore problematic for waste disposal.[8] Extensive research is made on carbon-based quantum dots, but the optical properties are still lacking compared to traditional QDs.[9] Conjugated polymers (CP) are also interesting fluorophores for applications such as fluorescence-based LFI signal transducers because of their extraordinary optical properties.[10]

Due to the inherent hydrophobicity of CPs, they can either be precipitated under controlled conditions to form NPs or can be encapsulated within the matrix of NP-forming materials.[11–17] The resulting conjugated polymer nanoparticles (CPN) exhibit favourable optical properties, a high colloidal stability and options for surface functionalisation, such as antibody conjugation.[18] One interesting method for CP encapsulation was

[a]*Institute of Pharmacy, Martin-Luther-University Halle-Wittenberg, Halle, Germany*
[b]*Institute of Biochemistry and Biotechnology, Martin-Luther-University Halle-Wittenberg, Halle, Germany*
[c]*Department of Physics, King's College London, London, UK. E-mail: leaann.dailey@univie.ac.at*
[d]*Department of Pharmaceutical Science, University of Vienna, Vienna, Austria*

† Electronic supplementary information (ESI) available. See DOI: 10.1039/d1ra05212h

reported by Tan *et al.* (2012), where the CP is encapsulated within in a poloxamer (Pluronic© F-127) micelle that is subsequently stabilised by a cross-linked silica shell which forms around the inner hydrophobic core of the particle (Si-NP).[19] To facilitate surface functionalisation, the poloxamer was functionalised with carboxy groups and conjugated to the amine group of folic acid, which resulted in CPN which could be used for targeted cell imaging. In the current study, this strategy was adopted for the surface modification of CP-loaded Si-NP with the model antibody, rabbit IgG, to assess for suitability in an enzyme-linked immunosorbent assay (ELISA)-like and lateral flow immunoassay (LFI) assay format.

The successful use of CPN in an LFI assay format was only recently reported by Fang *et al.* (2018).[20] In an assay for simultaneous detection of three different tumour markers three different CP emitting at different wavelengths, PF-TC6FQ (red), PFCN (green) and PFO (blue), were used simultaneously to distinguish between each of the individual tumor markers. In the study by Fang and co-authors, the CPN were formed *via* controlled co-precipitation with an amphiphilic polymer, comprised of a polystyrene backbone, grafted with carboxylic acid-terminated polyethylene groups (PS-*g*-PEG-COOH), into an aqueous medium. The carboxy-moieties were used to modify the CPN surface with antibodies raised against the specific tumour marker. A similar preparation technique had been previously reported in the literature by Wu *et al.* (2010), who described such CPN as polymer dots (Pdots), in reference to quantum dots. Therefore, the term will be used in the current study as well.[21] Importantly, Fang *et al.* demonstrated that the use of Pdots as LFI signal transducers could result in a limit of detection (LOD) for the prostate specific antigen (PSA) of 2.05 pg mL^{-1}. In contrast, the published LOD values of Au-NP LFI for PSA range from 0.2–10 ng mL^{-1}.[22–25]

While Fang *et al.* were the first to demonstrate the use of CPN in an LFI assay format, the sheer variety of CP with different optical properties as well as different possible nanoparticle architectures, opens up a wide field of study with regard to the implementation of CPN in LFI systems. For example, can the use of alternative CPs or nanoparticle formulations increase assay sensitivity? These two parameters were addressed in the current study, whereby two different CPs were chosen for investigation (Fig. 1).

PDOF, a CP with a small Stokes shift but very high extinction coefficient and quantum yield (QY) or brightness, was compared with CN-PPV, a polymer with a large Stokes shift but only moderate brightness. Both CPs were formulated as Si-NP and Pdots to investigate CP properties and nanoparticle architecture on the performance in immunoassays, such as ELISA and LFI. The emission spectrum of PDOF largely overlaps with the absorption spectrum of CN-PPV. Therefore, the combination of PDOF and CN-PPV within the Pdot architecture was explored to investigate whether an enhanced signal could be achieved through the effect of Förster resonance energy transfer (FRET) from PDOF to CN-PPV.[26–28] All CPN systems were compared directly to Au-NP, as well as commercially available polystyrene NP (PS-NP) loaded with a small molecule fluorophore to ascertain the gain in sensitivity of the CPN signal transducers compared with a visual read-out (Au-NP) and a reference fluorophore (PS-NP).

The results generated demonstrate a clear advantage of CPN in general compared to other signal transducers, including small molecule fluorophores. The FRET-enhanced CP blends show enhanced signal–background ratios (SBR) at higher CPN masses but are similar in performance to the single CP signal transducers at low NP mass values. Since optimisation of the FRET-enhanced CP blends was beyond the scope of the present study, future work focused on the FRET-based signal transducer systems is likely to result in a further reduction in test sensitivity.

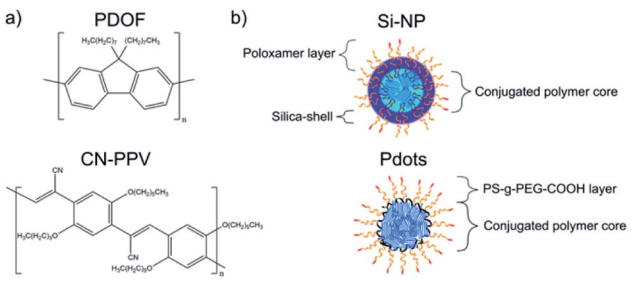

Fig. 1 Structure of conjugated polymers PDOF and CN-PPV (a) and of Si-NP and Pdots (b).

Methods

Materials

Poly-(9,9-di-*n*-octyl-fluorenyl-2,7-diyl) (PDOF), poly-(2,5-di-hexyloxy-cyanoterephthalylidene) (CN-PPV), rabbit IgG from rabbit serum, anti-rabbit IgG produced in goat and colloidal gold (Au-NP) 40 nm in 0.1 mM PBS were bought from Sigma-Aldrich. Polystyrene-*graft*-(ω-carboxylic acid polyethylene glycol) (PS-*g*-PEG-COOH) with M_n(PS)-*g*-M_n(PEG) = 6 kDa-*g*-3.7 kDa and 10 branches of PEG per PS backbone was acquired from Polymer sources, CA. Fluoresbrite® BB carboxylate microspheres 0.05 μm (PS-NP) were from Polysciences Europe. The Spectra/POR 6 dialysis membrane was acquired from Spectrumlabs. The LFI components Immunopore RP (NC membrane) and CF6 (wicking pad) were from GE Healthcare Life Sciences, UK.

Carboxylation of Pluronic© F127

The preparation of carboxylated Pluronic© F127 was done according to the method published by Tan *et al.*[19] (Yield = 51%) ^{1}H NMR (400 MHz, $CDCl_3$) δ = 4.26 (m, 4H, –COO–CH_2–), 3.64 (m, 400H, –CH_2–CH_2–), 3.54 (m, 112H, –CH_2–CH–), 3.39 (m, 56H, –C*H*–), 2.64 (m, 8H, –OOC–CH_2–CH_2–COO–), 1.14 (s, 168H, –CH_3) ppm (Fig. S2†).

Si-NP preparation

Si-NP preparation was adapted from Tan *et al.* with minor changes.[19] Briefly, Pluronic© F127 (80 mg) and F127–COOH (20 mg) was mixed with a solution of the CP in THF (*i.e.* 15, 200 and 500 μL for loading doses of 0.1, 2 and 4%, respectively, 5 g L^{-1}) and THF was added to a total volume of 1.2 mL. The mixture was heated to 45 °C and

stirred for 30 min. The solution was cooled to room temperature and tetramethoxysilane (65 μL) was added while stirring. The mixture was rapidly injected in deionised water (10 mL) under ultrasonication and sonicated for 13 min. The suspension was stirred in an open flask for 4 days in a low-airflow environment to complete hydrolysis and to evaporate the THF. Following evaporation, the mixture volume was replenished to 10 mL with deionised water and filtered through a 0.2 μm syringe filter to remove large particulates. Si-NP without F127–COOH were prepared with 100 mg Pluronic© F127 instead. To remove excess surfactant, 5 mL of the NP suspension were transferred into a centrifuge filter tube with MWCO = 100 kDa and 10 mL water were added. The mixture was reduced to 2 mL by ultrafiltration and water added to a total suspension volume of 15 mL. The filtration procedure was repeated three times and water added to a final volume of 5 mL. 1 mL of the crude and washed suspension was pipetted in previously weighted centrifuge tubes, freeze dried and weighted again to calculate the total solids content. The NP yield was calculated as total solids content divided by theoretical total solids content.

Pdot preparation

The preparation of Pdots was performed according to Fang *et al.* with minor changes.[20] Briefly, PDOF, CN-PPV or a 1 : 1 mixture of both in THF (*i.e.* 9.2, 96 and 200 μL for loading doses of 4, 40 and 83%, respectively, 1 mg mL^{-1}) and PS-*g*-PEG-COOH in THF (*i.e.* 115, 72 and 20 μL for loading doses of 4, 40 and 83%, respectively, 2 mg mL^{-1}) were mixed together in 5 mL THF. The mixture was sonicated for 15 s and subsequently injected into 10 mL of water under sonication. THF was removed by heating the mixture to 70 °C and purging with dry nitrogen for 25 min. The suspension was cooled to room temperature and deionised water was added to a final volume of 10 mL. The mixture was slowly filtered through a 0.22 μm syringe filter to remove dust and precipitated polymer.

Physicochemical characterisation: Si-NP, Pdots, PS-NP and Au-NP

The hydrodynamic diameter and zeta potential of NP was measured by DLS using the Malvern Zetasizer ZS Nano with a 633 nm laser and a scattering angle of 173°. The samples were diluted in deionised water to give a number of counts per second <150 000. The sizes reported are mean values of number distributions calculated by the Zetasizer Nano software v3.30. For zeta potential measurements 10 mM KCl was used as the electrolyte. The electrophoretic mobilities were transposed to zeta potentials by the Zetasizer Nano software using the Smoluchowski approximation.[29]

Characterisation of optical properties: Si-NP, Pdots and PS-NP

All measurements were performed using a Horiba FluoroMax 4 and quartz cuvettes with a light path length of 1 cm. The CP content of the NP suspensions was determined by absorption measurement using THF solutions of the polymers as calibration curve. For QY measurement the dispersions were diluted to optical density values between 0.05 and 0.1. Successively, emission spectra of the CP solutions and pure THF were recorded including the Rayleigh peak. The QY was calculated from the area under the curves of Rayleigh peaks (A_{Ex}, corresponding to the amount of absorbed photons) and emission peaks (A_{Em}, corresponding to the amount of emitted photons) according to eqn (1):[30]

$$\Phi = \frac{A_{Em}(CP) - A_{Em}(THF)}{A_{Ex}(THF) - A_{Ex}(CP)} \quad (1)$$

The values were internally corrected for wavelength-dependent reflectivity of the sphere by the evaluation software FluorEssence using a correction file specific to the integrating sphere used.

IgG conjugation of Si-NP, Pdots and PS-NP

NP suspension (40 μg NP), a solution of PEG400 in water (40 μL, 50 g L^{-1}) and HEPES buffer (40 μL, 1 M, pH = 7.4) were mixed and water was added to a total volume of 2 mL. Solutions of freshly prepared NHS in water (10 μL, 1 g L^{-1}) and EDC in water (40 μL, 1 g L^{-1}) were added and stirred for 5 min. A solution of rabbit IgG in water (367 μL, 36.7 μg, 0.1 g L^{-1}) was added and the mixture was stirred for 2 h at RT. A solution of BSA in water (10 μL, 100 μg, 10 g L^{-1}) was added and the suspension was stirred for 30 min. The resulting NP conjugate was purified by size exclusion chromatography (SEC) using Sephacryl 300-HR as stationary and HEPES buffer (20 mM, pH = 7.4) containing 1% PEG400 as mobile phase. The NP containing fractions were concentrated to 1 mL by ultrafiltration (MWCO = 100 kDa) and BSA (10 mg) was added.

Adsorption of IgG to the Au-NP surface

Au-NP were surface-modified with rabbit IgG according to literature.[31] Briefly, rabbit IgG (12.45 μg, 83 pmol) in borate buffer (100 μL, 2 mM, pH = 9) were mixed with a gold NP suspension (1.25 mL, 0.15 pmol, 58.2 μg) in borate buffer (0.25 mL, 2 mM, pH = 9) for 2 min. The suspension was centrifuged (3220 × *g*, 4 °C, 30 min), the upper layer was removed and the Au-NP were redispersed in PBS (1 mL) containing BSA (10 mg) and sodium azide (0.5 mg).

Fluorescence-linked immunosorbent assay (FLISA) of IgG-NP conjugates

Anti-rabbit IgG in 0.1 M borate buffer (50 μL, 1 μg, 20 μg mL^{-1}, pH = 9) was pipetted into wells of a 96-well plate. The plate was covered with parafilm and incubated at 4 °C overnight. The coating solution was removed and the wells were washed twice with 200 μL PBS containing 0.05% (w/w) Tween 20 (PBST). Remaining binding sites were blocked by adding a solution of BSA in PBS (150 μL, 50 g L^{-1}), covering with parafilm and incubating for 2 h at room temperature. The plate was washed twice with 200 μL PBST. IgG-NP-conjugate diluted in PBST containing 1 mg mL^{-1} BSA (100 μL, 3, 2, 1, 0.5, 0.1 and 0 mg L^{-1} or 300, 200, 100, 50, 10 and 0 ng) was added. The plate was covered with parafilm, incubated at room temperature for 2 h then washed three times with 200 μL PBST and filled with 200 μL PBST. Blank wells were prepared without addition of anti-

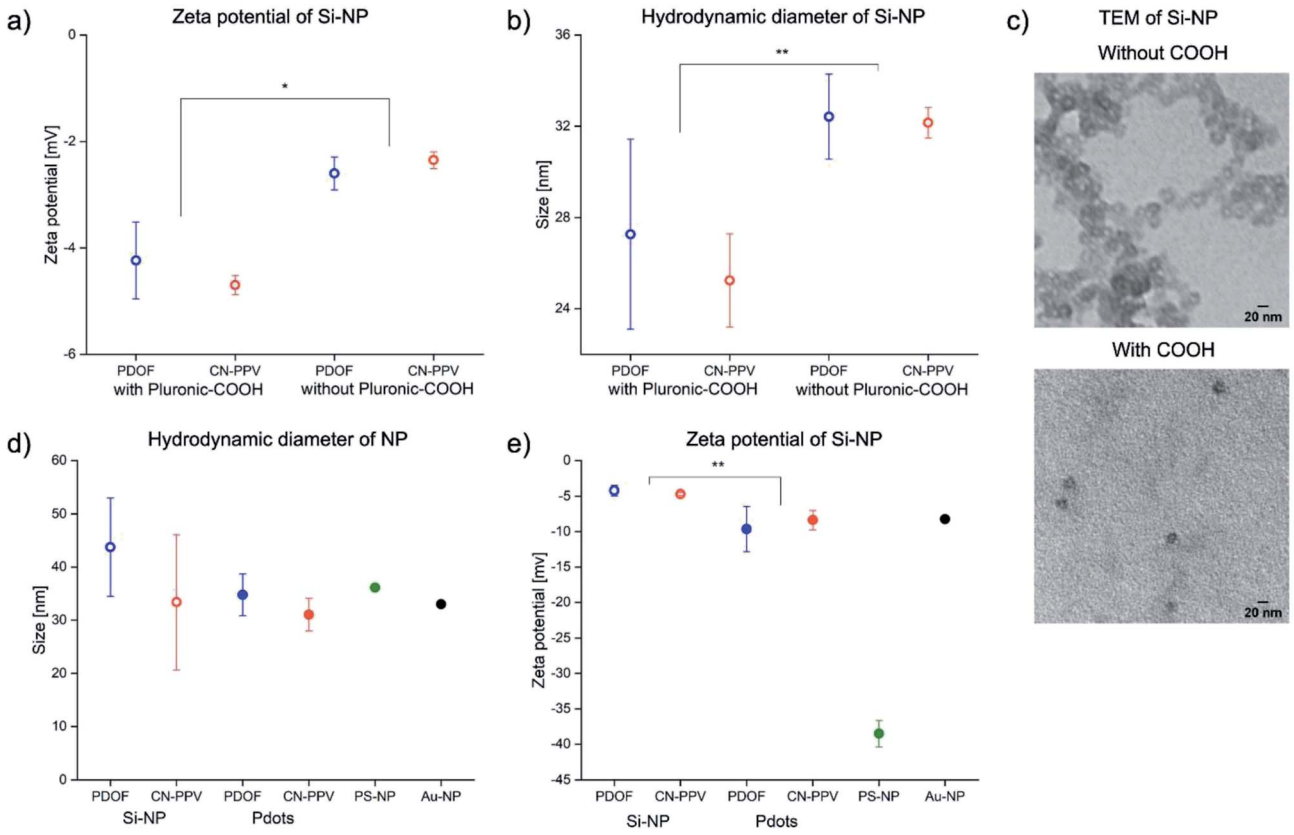

Fig. 2 Zeta potential (a), hydrodynamic diameter (b) and TEM images (c) of Si-NP prepared with and without carboxylated Pluronic© (CP loading dose = 0.1%). Hydrodynamic diameter (d) and zeta potential (e) for CPN and reference NP. (CP loading dose = 4% (Si-NP) and 83% (Pdots)) values represent mean ± standard deviation of $n = 3$ Si-NP and Pdot batches. One batch of PS-NP and Au-NP was measured in triplicate. *$p < 0.05$; **$p < 0.01$ (Welch-test).

rabbit IgG, but blocking with BSA in PBS (150 μL, 50 g L^{-1}). The signal intensities were measured with a Biotek Cytation 5 plate reader using the bottom optics. Si-NP, Pdots and PS-NP were measured in fluorescence endpoint/kinetic mode with a slit width of 20 nm and excitation/emission wavelengths of 378/437 nm (PDOF–Si-NP and –Pdots), 454/650 nm (CN-PPV–Si-NP and –Pdots) and 365/406 nm (PS-NP). The Au-NP were measured in absorption endpoint/kinetic mode at a wavelength of 534 nm. The signal : background ratio (SBR) was calculated as ratio of the mean intensity of wells containing capture antibody to the mean intensity of wells containing no capture antibody of same NP concentration.

LFI dipstick tests

Nitrocellulose membrane Immunopore RP (4 × 25 mm) was fixed on an adhesive plastic backing together with CF6 wicking pad (4 × 25 mm), overlapping 8 mm. A line of anti-rabbit IgG (0.2 g L^{-1}) with a width of 1 mm was drawn on the nitrocellulose membrane at a distance of 4 mm to the wicking pad with a fountain pen and the membrane dried for 10 min at room temperature. Wells of a 96-well plate were filled with a mixture of IgG–Pdot conjugates (10 μL), diluted to a conjugated polymer concentration of 2 μg mL^{-1} with HEPES buffer (20 mM, pH = 7.4) containing 1% PEG400, and a solution of 1% Triton X-100, 1% BSA and 1% PEG400 (50 μL). The strips were dipped in the mixture for 5 min and successively dried in vacuum at room temperature. The signal intensity was read with a QIAGEN LFReader at $\lambda_{Ex}/\lambda_{Em}$ = 365/430 nm (PDOF), 470/680 nm (CN-PPV) or 365/680 nm (PDOF–CN-PPV).

Results and discussion

NP preparation and characterisation

Si-NP and Pdots were produced by methods published by Tan *et al.* and Fang *et al.*[19,20] In contrast to Tan *et al.*, extensive purification of the Si-NP was used after preparation. This additional step was necessary to decrease the amount of free carboxylated Pluronic©, that would interfere in the subsequent conjugation reaction (Fig. S3†). The zeta potential of the Si-NP was neutral (−4 mV), in contrast to the electronegativity of the commercially available carboxylated PS-NP (−39 mV), indicating a higher density of carboxylic groups on the PS-NP surface.

Since the carboxylated Si-NP were expected to show a slightly greater electronegativity due to the presence of the modified poloxamer, the zeta potential of Si-NP prepared with non-carboxylated Pluronic© was also assessed. The comparison demonstrated that carboxylated Si-NP had a significantly

greater electronegative zeta potential ($P < 0.05$), indicating the presence of carboxylic groups on the Si-NP surface, albeit at a much lower density than PS-NP (Fig. 2a). Si-NP with non-carboxylated Pluronic© had larger hydrodynamic diameters due to a minor increase in core diameter (Fig. 2b and c). The NP were loaded with different amounts of CP (*i.e.* 0.1%, 1.6% and 4% for Si-NP and 4%, 40% and 83% for Pdots, respectively) to study the effect of loading dose (LD) on fluorescence brightness. A maximum of 4% LD could be used with Si-NP, as higher CP loading led to gelation of the NP dispersion. Pdots, in contrast, could be loaded with up to 83% CP without gelation, aggregation or sedimentation. At the highest loading dose, both CPN systems and the reference NP had comparable sizes of around 30 to 45 nm (Fig. 2d). In the literature, NP probes for LFI typically have sizes in the range from 15 nm to 800 nm.[32] Thus, both Si-NP and Pdots had suitable dimensions for LFI. The zeta potential for both CPN systems was −4 mV (Si-NP) and −10 mV (Pdots). Thus, carboxylic groups were present on the surface of NP with the highest loading dose, as well (Fig. 2e).

Optical characterisation

In THF solution, PDOF is a blue and CN-PPV a red emitter (Fig. 3a and b). In both nanoparticle formulations, PDOF and CN-PPV showed a red shift in emission compared to THF solution, as is commonly observed upon encapsulation.[33,34] The spectra of both CPN formulations were essentially identical, independent of whether Si-NP or Pdots were used as the NP architecture. The Stokes shift was much larger for CN-PPV (163–173 nm) than for PDOF (57–60 nm) (Table 1). The absorption spectrum of PDOF did not change upon encapsulation. The CN-PPV absorption red-shifted in Pdots and even further in Si-NP, compared to THF solution, as commonly observed for CN-PPV NP.[35] This solvatochromism is hypothesised to be caused by the negative inductive effect of the nitrile group which further

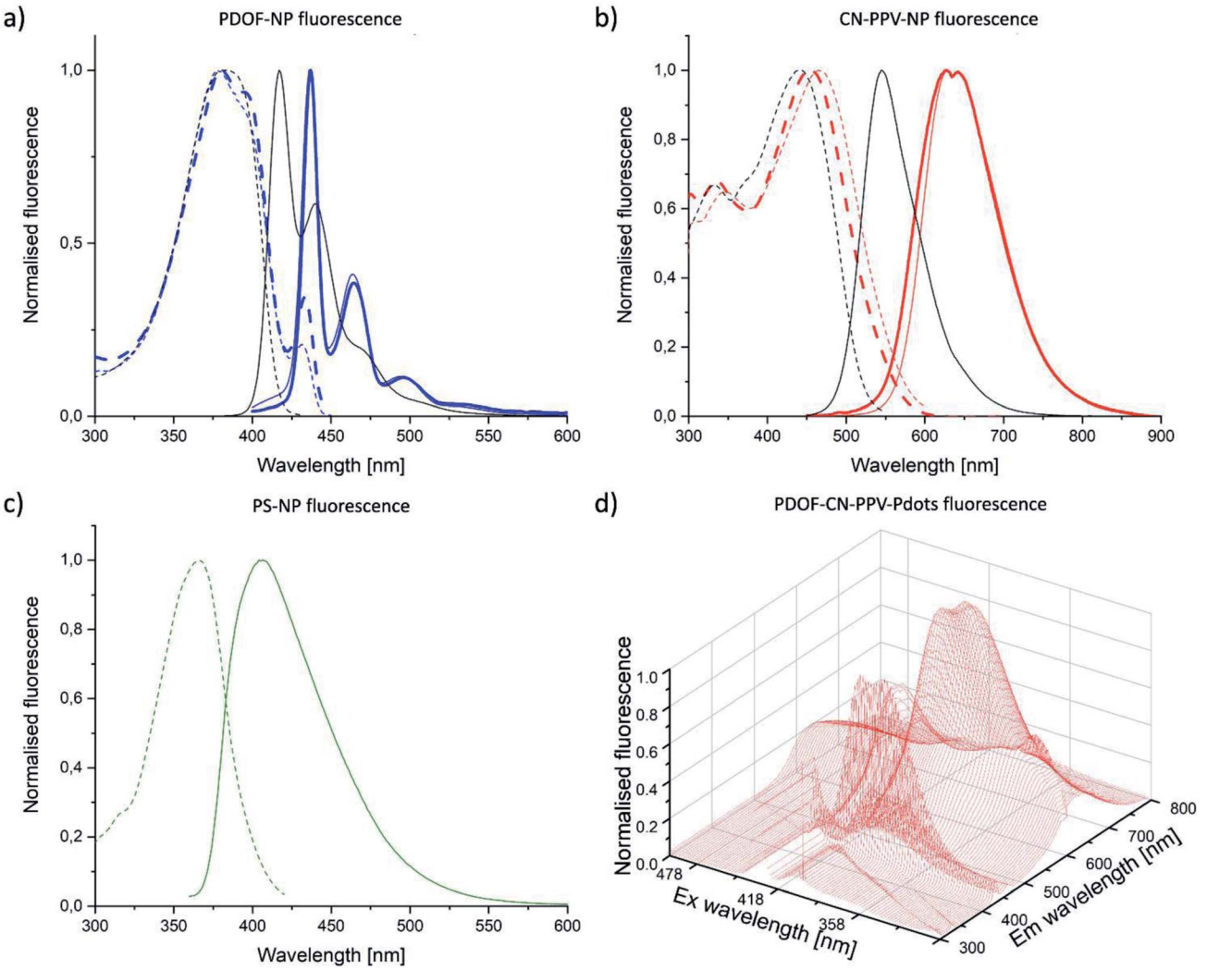

Fig. 3 Absorption (dashed lines) and fluorescence (solid lines) spectra of THF solution (black) or Si-NP (thin lines) and Pdots (thick lines) loaded with PDOF (a) or CN-PPV (b). Absorption (dashed line) and fluorescence (solid line) spectra of PS-NP (c). Combined absorption-emission spectra of PDOF–CN-PPV–Pdots (d). The Rayleigh peaks in the emission spectra of PDOF–CN-PPV–Pdots were removed by the evaluation software FluorEssence. CP loading doses were 4% (Si-NP) and 83% (Pdots).

Table 1 Comparison of optical properties of CP solution and CP NP. CP loading doses were 4% (Si-NP) and 83% (Pdots). CP concentration for QY measurement was 1 μg mL^{-1} (PDOF-NP) and 4 μg mL^{-1} (CN-PPV-NP). The same concentrations were used for measurement of CP solution spectra and QY

	CP	λ_{Ex} [nm]	λ_{Em} [nm]	$\Delta\lambda$ [nm]	φ [%]
THF solution	PDOF	381	417	36	98.6
	CN-PPV	442	545	103	17.7
Si-NP	PDOF	378	438	60	31.3 ± 5.0[a]
	CN-PPV	465	628	163	13.7 ± 2.6[a]
Pdots	PDOF	380	437	57	38.0 ± 7.2[a]
	CN-PPV	454	627	173	9.5 ± 0.9[a]
	PDOF–CN-PPV	380	627	247	>9.9[b]
PS-NP		366	406	40	64.8

[a] Mean ± standard deviation of 3 individual batches. [b] Emission ≥750 nm was not included in the calculation due to appearance of a scattering peak.

reduces electron density in polar solvents, therefore raising the electronic ground state.

The emission spectrum of a 1 : 1 (w/w) PDOF–CN-PPV polymer blend in Pdots displayed the sum of each individual emission spectrum when excited at the PDOF excitation wavelength, thus demonstrating energy transfer from PDOF to CN-PPV (Fig. 3d). The resulting Stokes shift of the blend was as large as 247 nm (Table 1). Moreover, the fluorescence intensity of the blend at the CN-PPV emission wavelength was much higher than that of CN-PPV alone. However, it is known that the FRET donor–acceptor ratio in CP blends influences the acceptor emission.[36] Fine-tuning of the blend composition could therefore further improve the optical properties. The excitation and emission bands of the reference PS-NP largely overlapped with PDOF-NP, thus allowing for detection of the reference nanoparticles with the same set of optical filters in the lateral flow reader used later in the study (Fig. 3c).

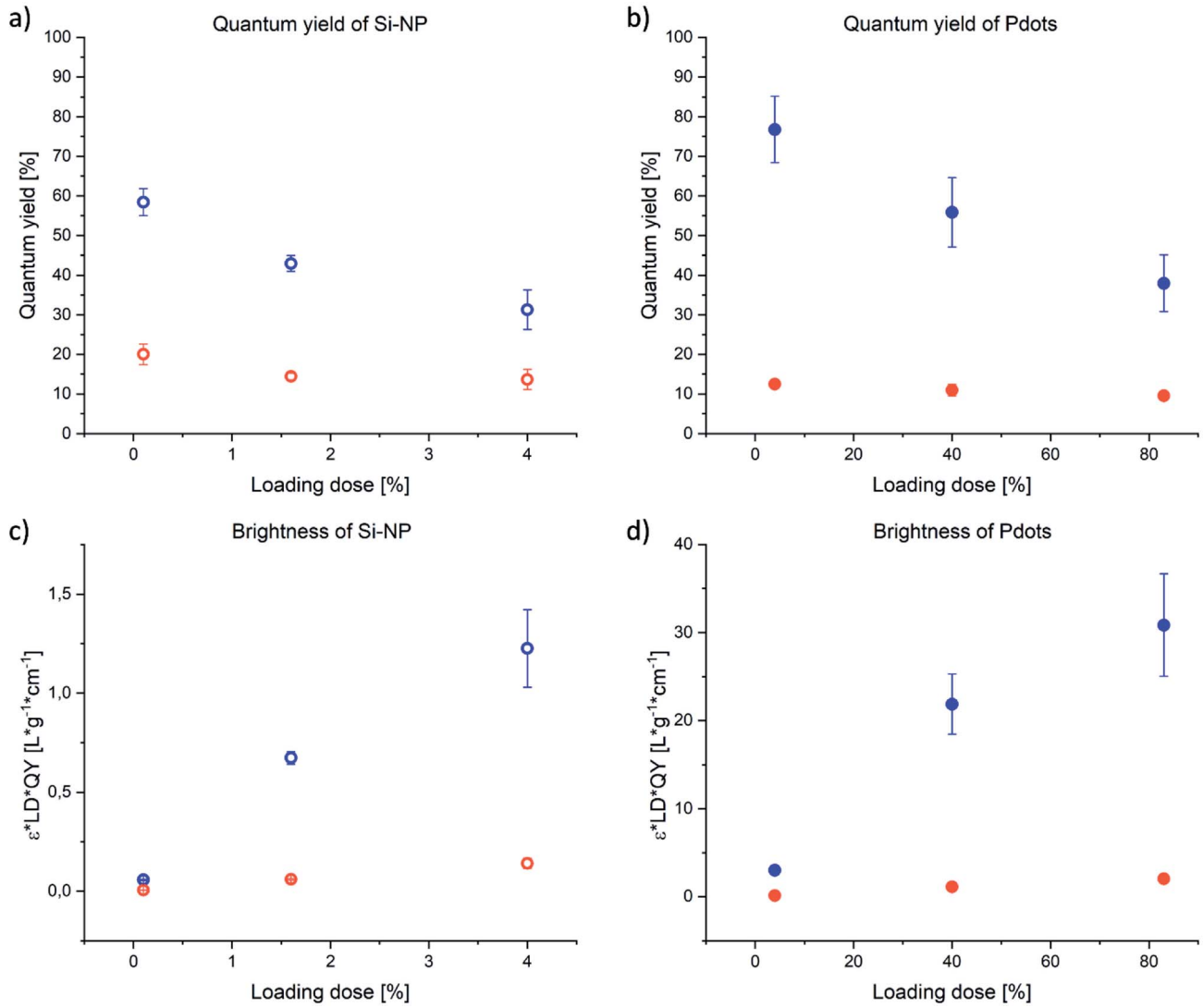

Fig. 4 QY (a and b) and brightness (c and d) of Si-NP (a and c) and Pdots (b and d) depending on CP loading dose of PDOF (blue) or CN-PPV (red). Values represent the mean ± standard deviation of $n = 3$ batches. The brightness was calculated according eqn (S7).†

The QY, in general, was much higher for the PDOF compared to CN-PPV CPN (Fig. 4). At the same loading dose (4%) the PDOF QY was significantly ($P < 0.01$) higher in Pdots (76.8%) than in Si-NP (31.3%), while the QY of CN-PPV was independent of nanoparticle architecture (12.5% (Pdots) and 13.7% (Si-NP)). In fluorescent dye solutions, the QY decreases with increasing dye concentration due to the inner filter effect.[37] Accordingly, the fluorescence QY decreased with increasing LD for both NP types and CP. However, the brightness of the NP increased with LD because of the higher absorbance. Due to the high QY and large extinction coefficient, the calculated brightness (see ESI†) of PDOF systems was 9–23 times higher than the CN-PPV CPNs (Fig. 4). The QY of the blend (>9.9%) was approximately the same as of CN-PPV–Pdots (9.5%) of the same loading dose (Table 1). However, the brightness was further increased because of the high extinction coefficient of the included PDOF (Fig. 4). The Si-NP and Pdots with the highest LD and therefore highest brightness, were taken forward to antibody conjugation and immunoassay studies.

Immunoassay performance – FLISA

Si-NP, Pdots and reference NP were conjugated to rabbit IgG as model antibody and subsequently tested for performance in two types of immunoassays: FLISA and LFI. The reaction conditions of conjugation were optimised for Pdots with respect to antibody amount and reaction pH (see ESI†). The FLISA format was used to compare the signal : background ratio (SBR) of the five different signal transducer systems independent of variables which can affect LFI performance, such as NP flow characteristics and interactions with LFI membranes.[38] Wells of a microwell plate were coated with anti-rabbit IgG as a capture antibody and incubated with dispersions containing different NP masses for 2 h, as reported to be sufficient time in NP-based ELISA.[39,40] Wells without capture antibody, but BSA coating only, were also incubated with all systems and used for background determination. The Pdot formulations had superior SBR compared to the Si-NP, PS-NP and Au-NP over the entire range tested (Fig. 5). As expected based on the calculated brightness values, the low-loading dose Si-NP showed lower SBR than high-loading dose Pdots with the same fluorophore. Interestingly, CN-PPV Pdots performed better than PDOF Pdots indicating that the brightness of NP had less of an impact on the SBR compared to Stokes shift. This is because the larger Stokes shift resulted in a greatly decreased background signal, which is an important practical consideration for both FLISA and LFI assay formats. Surprisingly, the Pdot system containing the CP blend did not significantly outperform the CN-PPV Pdot system (Fig. 5b) despite the 1.4-fold increase in Stokes shift (Table 1), although at higher NP mass values (>200 ng) the SBR of the Pdots with the CP blend was greater than that of the CN-PPV Pdots (Fig. 5b). These results may indicate that if the Stokes shift of the fluorophore is large enough to reduce the background signal, then the brightness of the fluorophore becomes an important factor. Although a brightness value for the blend is difficult to calculate, the QY values of the blend and the CN-PPV systems are perhaps close enough to explain their similar performance in the FLISA.

Immunoassay performance – dipstick LFI

To assess the performance of CP in a more complex lateral flow environment, the five signal transducers were investigated in dipstick LFI assay format. A dipstick LFI is similar to a conventional LFI but does not contain the nanoparticle signal

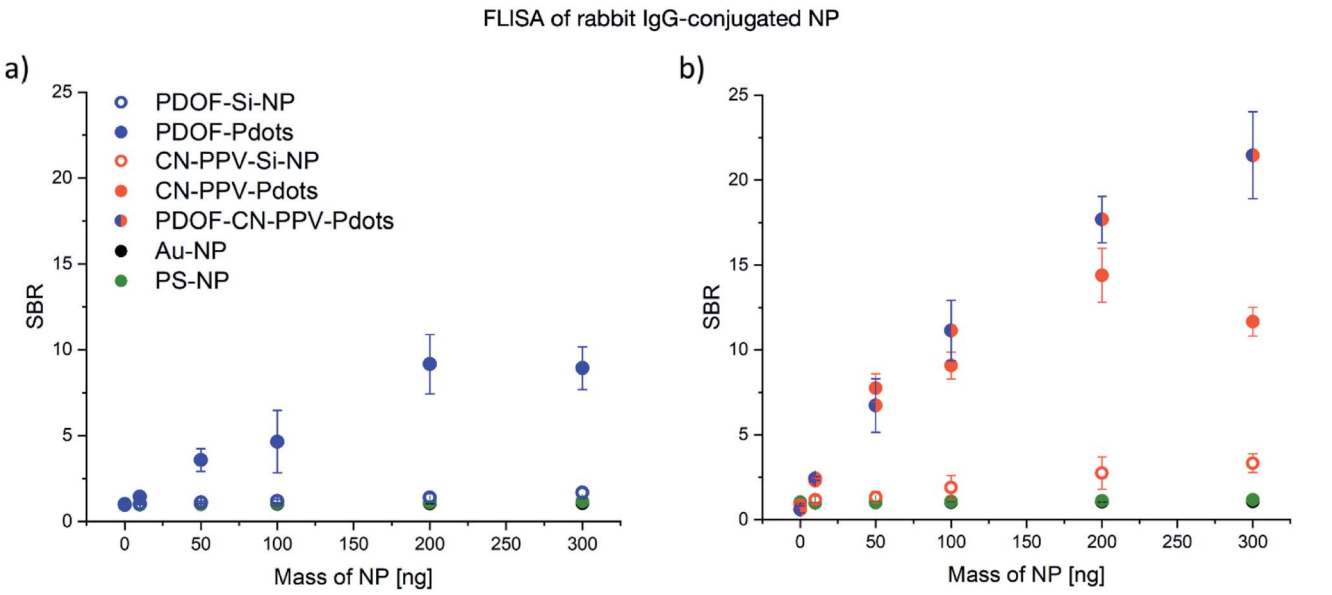

Fig. 5 Performance of NP-IgG-conjugates in a FLISA system. Signal-to-background ratio (SBR) of wells coated with capture Ab to wells coated only with BSA. Fluorescent readout of PDOF–Si-NP (blue open circle) and PDOF–Pdots (blue) (both $\lambda_{Ex}/\lambda_{Em} = 378/437$ nm) compared to PS-NP (green; $\lambda_{Ex}/\lambda_{Em} = 365/406$ nm) and Au-NP (black; $\lambda = 534$ nm) (a). CN-PPV–Si-NP (red open circle), CN-PPV–Pdots (red) (both $\lambda_{Ex}/\lambda_{Em} = 454/650$ nm) and PDOF–CN-PPV–Pdots (red-blue) ($\lambda_{Ex}/\lambda_{Em} = 378/650$ nm) compared to PS-NP (green) and Au-NP (black) (b). Values are mean ± standard deviation of means of 3 wells each on 3 plates.

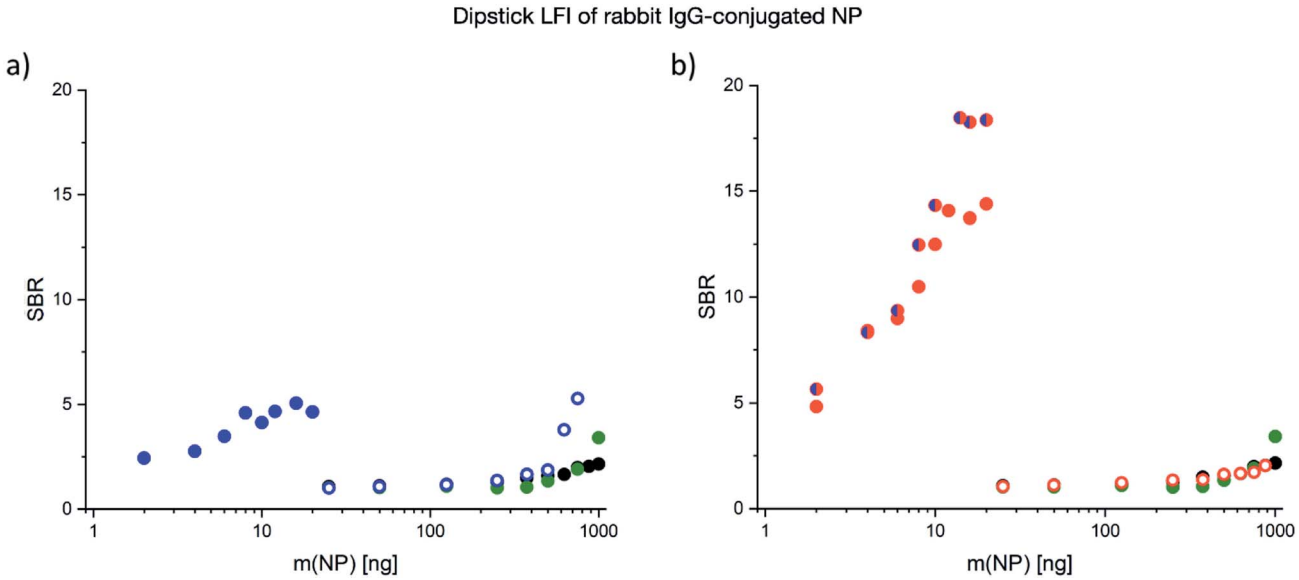

Fig. 6 SBR *versus* NP mass in dipstick-LFI of rabbit IgG-NP conjugates. PDOF–Si-NP (blue open circle) and PDOF–Pdots (blue) compared to PS-NP (green) and Au-NP (black) (a). CN-PPV–Si-NP (red open circle), CN-PPV–Pdots (red) and PDOF–CN-PPV–Pdots (blue-red) compared to PS-NP (green) and Au-NP (black) (b).

transducers in dry form within a reservoir pad. Instead, the membrane is dipped into the nanoparticle dispersion and allowed to flow unimpeded across the LFI membrane. Dipstick tests are often used in LFI development, because they reduce the level of complexity of the assay in the first instance. Two methods of signal detection were compared with each other in this investigation: (1) quantitative determination of the signal using a QIAGEN LFReader and (2) semi-quantitative image-based analysis of the visual read-out using a UV light box for illumination, a mobile phone for image capture and ImageJ software for image analysis. The first method provides a greater read-out sensitivity and accuracy, whereby the second method

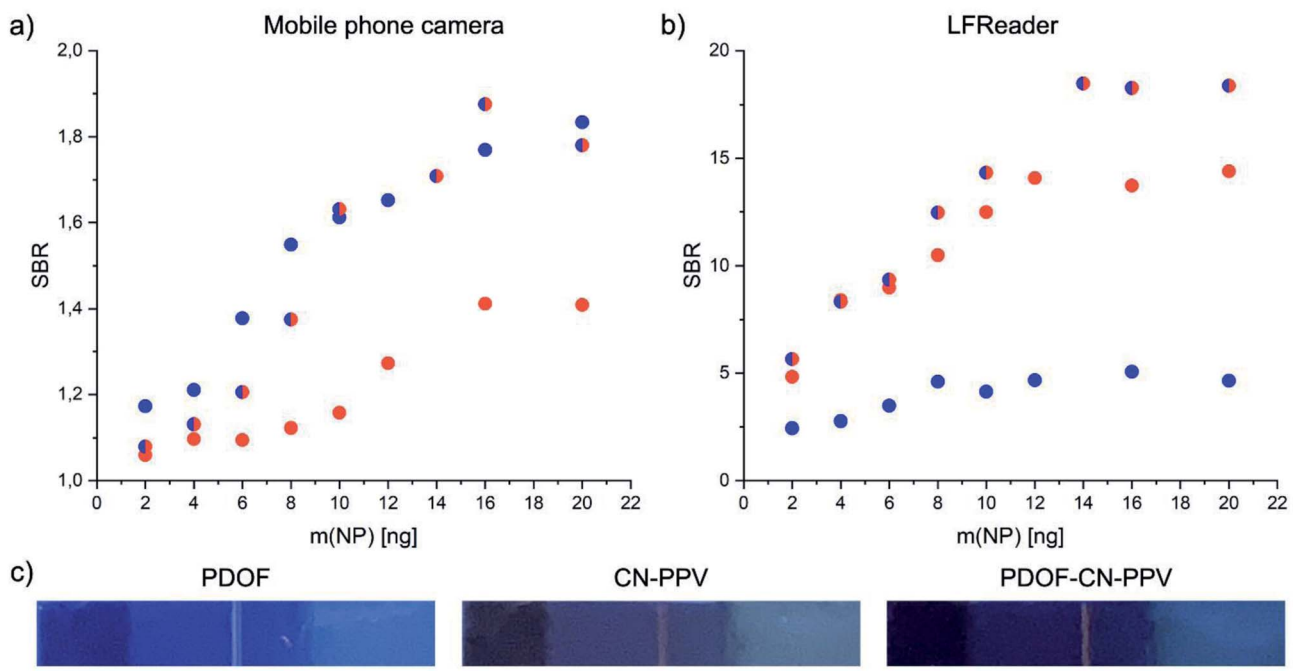

Fig. 7 A comparison of SBR determination using (a) a UV light box combined with mobile phone image acquisition compared to (b) a commercial LFReader system. The dipstick-LFI assay format was used to generate test strips containing Pdots of PDOF (closed blue circles), CN-PPV (closed red circles) and PDOF–CN-PPV blends (blue-red circles). (c) Representative images of the test strips used for image analysis are presented below for visual comparison.

can be used in environments which cannot invest in the more expensive LFI readers.

Using the QIAGEN LFReader for quantitative signal analysis, similar trends were observed in the dipstick LFI assay format compared with the FLISA results (Fig. 6). In general, the NP mass required for detection was two orders of magnitude lower for Pdots compared to Si-NP and the reference NP. Similar to the FLISA, the CN-PPV–Pdots showed a substantially higher SBR compared to PDOF Pdots. Furthermore, the CP blend Pdots showed a performance similar to the CN-PPV Pdots at lower nanoparticle masses, but superior SBR values at the higher masses tested. This difference is believed to be caused by the inner filter effect that is more pronounced at high fluorophore concentrations, but generally reduced for the CP blend particles, in which the effective concentration of each CP is reduced by half.

Because not all facilities have access to an LFReader, an alternative method of fluorescence detection using a UV light box, image capture with a mobile phone and image analysis using ImageJ software was implemented using only selected Pdot systems containing PDOF, CN-PPV and the blend. The results of this alternative mode of signal detection as compared to the LFReader are depicted in Fig. 7. As expected, the image acquisition with the mobile phone technology resulted in lower SBR values compared to the LFReader, due to the lower sensitivity of the detection method. Interestingly, the visual analysis of the test strip signals resulted in higher SBR values for Pdots comprised of PDOF and the CP blend compared to CN-PPV. This may be explained by the fact that the excitation wavelength of the UV light box was 365 nm and therefore optimal for PDOF excitation, but suboptimal for CN-PPV excitation. However, the results do demonstrate that visual assessment LFI assays employing CPN signal transducers is perhaps less sensitive to high background fluorescence and therefore less dependent on fluorophores with large Stokes shifts. In this case, the fluorophore brightness may represent the more influential factor. Based on these interesting first results, further studies investigating these parameters in greater depth are justified.

Conclusions

In this study, two CP polymers and a 1 : 1 blend were formulated into NPs with two distinct architectures: Si-NP and Pdots. The resulting five CPN systems were directly compared to commercially available PS-NP of a similar size loaded with a small-molecule fluorescent dye and colloidal gold for their performance in two types of immunoassays. The resulting data support the hypothesis that CP-based fluorophores dramatically increase the sensitivity of the immunoassays investigated, often by 1–2 fold magnitudes of order when expressed as mass of nanoparticles binding to the capture antibody necessary to achieve a significant SBR. The results showed that the Pdot architecture was superior to the Si-NP architecture in all cases, due to the higher CP loading dose achievable and the greater colloidal stability. It was also important to observe that CPNs with a greater Stokes shift achieved a significantly higher SBR in both the FLISA and LFI assay formats, likely due to a reduced background fluorescence. FRET-based Pdots containing a CP blend showed excellent performance, especially at higher nanoparticle concentrations, but were not superior to CN-PPV Pdots at lower nanoparticle masses. This information indicates that the choice of an acceptor CP with both a large Stokes shift and higher brightness might achieve further improvements to the SBR of FRET-based signal transducers and indicates a promising course for future studies. Finally, the comparison of an inexpensive method of detection utilizing a UV light box combined with mobile phone image acquisition demonstrated that Pdots can be used as LFI signal transducers with a visual readout. Although the SBR values are lower than those generated using a LFReader, this data demonstrates a way to extend the range of use of fluorescence-based LFIs to areas where low cost technologies are required.

Conflicts of interest

There are no conflicts to declare.

Acknowledgements

This work was supported by the “European Regional Development Fund” (ERDF 2016–2023), Project: ZS/2016/08/80590.

References

1 World Health Organization, *Weekly Epidemiological Update on COVID-19*, https://www.who.int/docs/default-source/coronaviruse/situation-reports/20201012-weekly-epi-update-9.pdf, accessed 17 January 2021.
2 P. Pokhrel, C. Hu and H. Mao, *ACS Sens.*, 2020, **5**, 2283–2296.
3 A. Scohy, A. Anantharajah, M. Bodéus, B. Kabamba-Mukadi, A. Verroken and H. Rodriguez-Villalobos, *J. Clin. Virol.*, 2020, **129**, 104455.
4 W. C. Mak, V. Beni and A. P. F. Turner, *TrAC, Trends Anal. Chem.*, 2016, **79**, 297–305.
5 Food and Drug Administration, *In Vitro Diagnostics EUAs*, https://www.fda.gov/medical-devices/coronavirus-disease-2019-covid-19-emergency-use-authorizations-medical-devices/vitro-diagnostics-euas, accessed 19 January 2021.
6 J. Li and J. J. Zhu, *Analyst*, 2013, **138**, 2506–2515.
7 A. F. Holleman, N. Wiberg and E. Wiberg, *Lehrbuch der Anorganischen Chemie*, Walter de Gruyter, Berlin, 102nd edn, 2007.
8 R. Hardman, *Environ. Health Perspect.*, 2006, **114**, 165–172.
9 Y. Liu, H. Huang, W. Cao, B. Mao, Y. Liu and Z. Kang, *Mater. Chem. Front.*, 2020, **4**, 1586–1613.
10 J. Pecher and S. Mecking, *Chem. Rev.*, 2010, **110**, 6260–6279.
11 C. Wu, B. Bull, C. Szymanski, K. Christensen and J. McNeill, *ACS Nano*, 2008, **2**, 2415–2423.
12 C. Wu, S. J. Hansen, Q. Hou, J. Yu, M. Zeigler, Y. Jin, D. R. Burnham, J. D. McNeill, J. M. Olson and D. T. Chiu, *Angew. Chem., Int. Ed.*, 2011, **50**, 3430–3434.
13 H. Y. Liu, P. J. Wu, S. Y. Kuo, C. P. Chen, E. H. Chang, C. Y. Wu and Y. H. Chan, *J. Am. Chem. Soc.*, 2015, **137**, 10420–10429.

14 M. Green, P. Howes, C. Berry, O. Argyros and M. Thanou, *Proc. R. Soc. A*, 2009, **465**, 2751–2759.
15 C. Kim, S. Y. Kim, Y. T. Lim and T. S. Lee, *Macromol. Res.*, 2017, **25**, 572–577.
16 P. R. Neumann, D. L. Crossley, M. Turner, M. Ingleson, M. Green, J. Rao and L. A. Dailey, *ACS Appl. Mater. Interfaces*, 2019, **11**, 46525–46535.
17 P. Modicano, P. R. Neumann, M. Schüller, J. Holthof, F. L. Kyrilis, F. Hamdi, P. L. Kastritis, K. Mäder and L. Ann Dailey, *Eur. J. Pharm. Biopharm.*, 2020, **154**, 297–308.
18 K. Li and B. Liu, *J. Mater. Chem.*, 2012, **22**, 1257–1264.
19 H. Tan, Y. Zhang, M. Wang, Z. Zhang, X. Zhang, A. M. Yong, S. Y. Wong, A. Y. Chi Chang, Z. K. Chen, X. Li, M. Choolani and J. Wang, *Biomaterials*, 2012, **33**, 237–246.
20 C. Fang, C. Chou, Y. Yang, T. Wei-Kai, Y. Wang and Y.-H. Chan, *Anal. Chem.*, 2018, **90**, 2134–2140.
21 C. Wu, T. Schneider, M. Zeigler, J. Yu, P. G. Schiro, D. R. Burnham, J. D. McNeill and D. T. Chiu, *J. Am. Chem. Soc.*, 2010, **132**, 15410–15417.
22 C. Fernández-Sánchez, C. J. McNeil, K. Rawson, O. Nilsson, H. Y. Leung and V. Gnanapragasam, *J. Immunol. Methods*, 2005, **307**, 1–12.
23 R. Tanaka, T. Yuhi, N. Nagatani, T. Endo, K. Kerman, Y. Takamura and E. Tamiya, *Anal. Bioanal. Chem.*, 2006, **385**, 1414–1420.
24 I. A. Lubavina, A. A. Zinchenko, Y. S. Lebedin and S. V. Chukanov, *Russ. J. Bioorg. Chem.*, 2007, **33**, 511–515.
25 I. P. Andreeva, V. G. Grigorenko, A. M. Egorov and A. P. Osipov, *Anal. Lett.*, 2016, **49**, 579–588.
26 T. Klingstedt and K. P. R. Nilsson, *Biochim. Biophys. Acta, Gen. Subj.*, 2011, **1810**, 286–296.
27 J. S. Kim, P. K. H. Ho, C. E. Murphy and R. H. Friend, *Macromolecules*, 2004, **37**, 2861–2871.
28 T. Kietzke, D. Neher, K. Landfester, R. Montenegro, R. Güntner and U. Scherf, *Nat. Mater.*, 2003, **2**, 408–412.
29 J. D. Clogston and A. K. Patri, in *Characterization of Nanoparticles Intended for Drug Delivery*, ed. S. E. McNeil, Humana Press, Totowa, NJ, 2011, pp. 63–70.
30 K. L. Wong, J. C. G. Bünzli and P. A. Tanner, *J. Lumin.*, 2020, **224**, 117256.
31 S. Wiriyachaiporn, P. H. Howarth, K. D. Bruce and L. A. Dailey, *Diagn. Microbiol. Infect. Dis.*, 2013, **75**, 28–36.
32 G. A. Posthuma-Trumpie, J. Korf and A. Van Amerongen, *Anal. Bioanal. Chem.*, 2009, **393**, 569–582.
33 S. Bourke, L. Urbano, A. Olona, F. Valderrama, L. A. Dailey and M. A. Green, in *Reporters, Markers, Dyes, Nanoparticles, and Molecular Probes for Biomedical Applications IX*, ed. S. Achilefu and R. Raghavachari, 2017, vol. 10079, p. 100790A.
34 P. Koralli, A. D. Nega, L. E. Vagiaki, A. Pavlou, M. G. Siskos, A. Dimitrakopoulou-Strauss, V. G. Gregoriou and C. L. Chochos, *Mater. Chem. Front.*, 2020, **4**, 2357–2369.
35 R. Peters, L. Sandiford, D. M. Owen, E. Kemal, S. Bourke, L. A. Dailey and M. Green, *Photochem. Photobiol. Sci.*, 2016, **15**, 1448–1452.
36 C. Pan, K. Sugiyasu and M. Takeuchi, *Chem. Commun.*, 2014, **50**, 11814–11817.
37 J. R. Lakowicz, *Principles of Fluorescence Spectroscopy*, Springer US, Boston, MA, 2006.
38 E. B. Bahadır and M. K. Sezgintürk, *TrAC, Trends Anal. Chem.*, 2016, **82**, 286–306.
39 L. Zhan, W. B. Wu, X. X. Yang and C. Z. Huang, *New J. Chem.*, 2014, **38**, 2935–2940.
40 M. M. Billingsley, R. S. Riley and E. S. Day, *PLoS One*, 2017, **12**, 1–15.